

A class of uniaxial phenomenological models for simulating hysteretic phenomena in rate-independent mechanical systems and materials

Nicolò Vaiana  · Salvatore Sessa ·
Francesco Marmo · Luciano Rosati

Received: 30 November 2017 / Accepted: 4 April 2018
© Springer Science+Business Media B.V., part of Springer Nature 2018

Abstract We present a general formulation of a class of uniaxial phenomenological models, able to accurately simulate hysteretic phenomena in rate-independent mechanical systems and materials, which requires only one history variable and leads to the solution of a scalar equation for the evaluation of the generalized force. Two specific instances of the class, denominated Bilinear and Exponential Models, are developed as an example to illustrate the peculiar features of the formulation. The Bilinear Model, that is one of the simplest hysteretic models which can be emanated from the proposed class, is first described to clarify the physical meaning of the quantities adopted in the formulation. Specifically, the potentiality of the proposed class is witnessed by the Exponential Model, able to simulate more complex hysteretic behaviors of rate-independent mechanical systems and materials exhibiting either kinematic hardening or softening. The accuracy and the computational efficiency of this last model are assessed by carrying out nonlinear time history analyses, for a single degree of freedom mechanical system having a rate-independent kinematic hardening behavior, subjected either to a harmonic or to a random force. The relevant results are compared with those obtained by exploiting the widely used Bouc–Wen Model.

Keywords Mechanical hysteresis · Phenomenological model · Hardening · Softening

1 Introduction

Hysteresis is a widespread phenomenon in science and engineering playing a significant role in industrial and technological applications.

Generally, the output of a hysteretic system depends on the past history of the input besides its current value, so that a number of state variables need to be known. Hysteresis is usually termed dynamic or static whether the rate of variation of the input does or does not influence the output [16]. Equivalent denominations are rate-dependent hysteresis in the former case and rate-independent in the latter.

Magnetics and mechanics are the two main areas of science and engineering where hysteresis phenomena are observed [64]. Hysteresis occurring in soft or hard magnetic systems and materials, such as soft iron, Si steel, permalloy, hexagonal ferrites, and Nd–Fe–B [6, 13], is referred to as magnetic hysteresis, whereas hysteresis occurring in mechanical systems and materials, such as ductile metals [67] and geomaterials [4], is referred to as mechanical hysteresis.

Hysteretic phenomena are so complex that they cannot be satisfactorily described by a single universal model. Indeed, the spectrum of their applications is so broad and their origin is due to such sophisticated

N. Vaiana (✉) · S. Sessa · F. Marmo · L. Rosati
Department of Structures for Engineering and Architecture,
University of Naples Federico II, Via Claudio, 21, 80124
Naples, Italy
e-mail: nicolovaiana@outlook.it

and still unclear physical mechanisms that many phenomenological models have been proposed in the past.

Basically, phenomenological models are mathematical models that do not try to shed light on the physical origin of hysteresis but, rather, try to provide a suitable description and generalization of experimental findings [41]. Nevertheless, they have been resorted to, in the past as well as at present times, as powerful tools for design purposes.

As regards the hysteresis modeling of magnetic systems and materials, some of the widely used models are the Preisach model [41], the Jiles–Atherton model [31,32], the Energetic Hauser model [26], and the Coleman–Hodgdon model [27]. As far as the hysteresis modeling of mechanical systems and materials is concerned, some of the widely used models are the bilinear model [1, 11, 19, 68], the Bouc–Wen model [8, 65, 66], the Ozdemir model [45], the Ramberg–Osgood model [49], the Giuffrè–Menegotto–Pinto model [23, 42], and plasticity-based models, such as multilayer models [7], single surface models [38], two-surface models [14, 15, 34], multi-surface models [29], and parallel elasto-plastic models [43].

Most of the existing phenomenological models, initially developed to describe a particular type of hysteresis, have been subsequently extended to describe other types of hysteretic phenomena, with their mathematical forms being suitable for multi-disciplinary extensions. For instance, hysteresis induced by friction occurring between several mechanical components of systems has been successfully described by the Preisach model [16].

A comprehensive classification of the hysteretic models is a rather hard task due to their large number. This is usually performed in the literature depending on the kind of equations that mathematically characterize the output variables. Actually, it is possible to distinguish:

- algebraic models, such as the bilinear, Ramberg–Osgood [49], and Giuffrè–Menegotto–Pinto [23, 42] models, in which an algebraic equation is solved to compute the output;
- transcendental models, in which the output is computed by solving transcendental equations, such as the Energetic Hauser model [26]. Transcendental equations involve functions such as trigonometric, inverse trigonometric, exponential, logarithmic, and hyperbolic functions [56];

- differential models, such as the Jiles–Atherton [31,32], Coleman–Hodgdon [27], Bouc–Wen [8, 65, 66], and Ozdemir [45] models, in which first- or higher-order differential equations, either of ordinary or partial type, are solved to evaluate the output;
- integral models, such as the Preisach model [41], characterized by equations expressed in integral form.

The above-mentioned models can be broadly classified into two large categories. Actually, the current values of the input and output variables, as well as the direction of variation of the input variable, generally suffice to fully describe the behavior of hysteretic systems by exploiting differential models.

Conversely, the last reversal point of the hysteretic response, the direction along which input variation is considered, as well as additional information on the system history, is generally taken into account by algebraic, transcendental, and integral models.

This paper presents a class of uniaxial phenomenological models able to simulate hysteresis loops, limited by two parallel straight lines or curves, typical of rate-independent mechanical systems and materials with kinematic hardening or softening hysteretic behavior. The proposed class of models offers several important advantages over hysteretic models generally adopted to simulate the mechanical hysteresis phenomena. Actually, compared to differential models, the proposed class does not exploit the numerical solution of a differential equation, generally solved by adopting multi-steps [48] or Runge–Kutta methods [50], with the remarkable benefit of very significantly reducing the computational effort of finite element analyses. Compared to plasticity-based models, the proposed class of hysteretic models does not require the use of a return map algorithm [53] and can be easily implemented in a computer program.

The present paper is organized into three parts. In the first part (Sect. 2), the rate-independent hysteretic behavior of mechanical systems and materials, endowed with kinematic hardening or softening, is shortly described. In the second part (Sects. 3 and 4), the general formulation of the class of models is first presented. To better illustrate the features of the general formulation, always leading to the evaluation of the generalized force by solving a scalar equation, two specific instances of the proposed class, denom-

inated Bilinear Model and Exponential Model, are presented. In particular, making reference to the classification alluded to above, the former is an algebraic model whereas the latter is a transcendental one since this characterizes, from a mathematical point of view, the nature of the scalar equation that provides the generalized force. The Bilinear Model is first illustrated to easily describe the meaning of the adopted quantities, since it represents one of the simplest models that can be emanated from the proposed class, whereas the Exponential Model is presented to illustrate the potentialities of the class, since it is able to accurately simulate a wide spectrum of rate-independent mechanical systems and materials.

In the third part (Sect. 5), the accuracy and the computational efficiency of the more elaborate Exponential Model are assessed by carrying out some nonlinear time history analyses performed on a rate-independent kinematic hardening post-yield single degree of freedom mechanical system. In particular, the results obtained for two different external forces, that is, a harmonic and a random force, have been compared with those obtained by using the celebrated Bouc–Wen Model [8,65,66], one of the most used differential models in the literature [2,3,17,25,33,35,36,44].

2 Rate-independent mechanical systems and materials

Mechanical hysteresis is a rate-dependent or rate-independent process having a generalized displacement u , that is, displacement, rotation or strain as input, and a generalized force f , that is, force, moment or stress as output, or vice versa. In actual mechanical systems and materials, both types of hysteretic phenomena can be observed at the same time, although only rate-independent mechanical hysteresis is considered in this paper.

In rate-independent mechanical systems and materials, hysteresis is generally induced by plastic deformation mechanisms and/or friction forces [47]. If the generalized displacement cycles between two values, the generalized force traces a hysteresis loop in the input–output plane. This behavior is characterized by kinematic hardening (softening) when the generalized force increases (decreases) with generalized displacement and the hysteresis loops are limited by two bounds, i.e., two parallel limiting straight lines or curves, whose

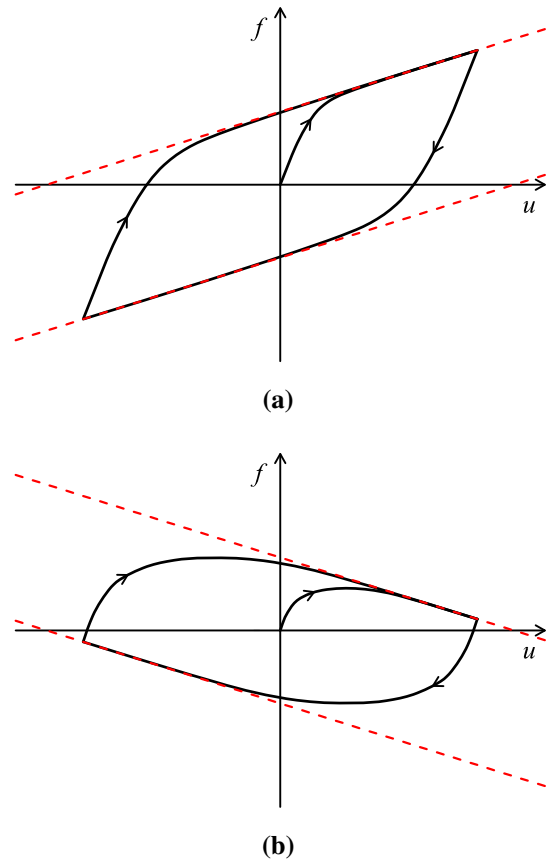


Fig. 1 An example of hysteresis loop limited by two straight lines typical of mechanical systems and materials exhibiting kinematic hardening (a) and softening (b) behavior

distance remains constant under repeated cycles. The increasing (decreasing) values of generalized forces as function of increasing values of generalized displacements, which typically characterizes hardening (softening), do not have to be confused with the behavior of the generalized tangent stiffness df/du whose value is positive (negative) when hardening (softening) occurs.

As an example of the aforementioned behaviors, Figs. 1a, 2a shows a hysteresis loop bounded by two straight lines (curves) typical of kinematic hardening mechanical systems and materials, whereas the hysteresis loop plotted in Figs. 1b, 2b is typical of kinematic softening behaviors.

In the field of structural, geotechnical, and seismic engineering, there are several examples of mechanical systems and materials having a rate-independent hysteretic behavior.

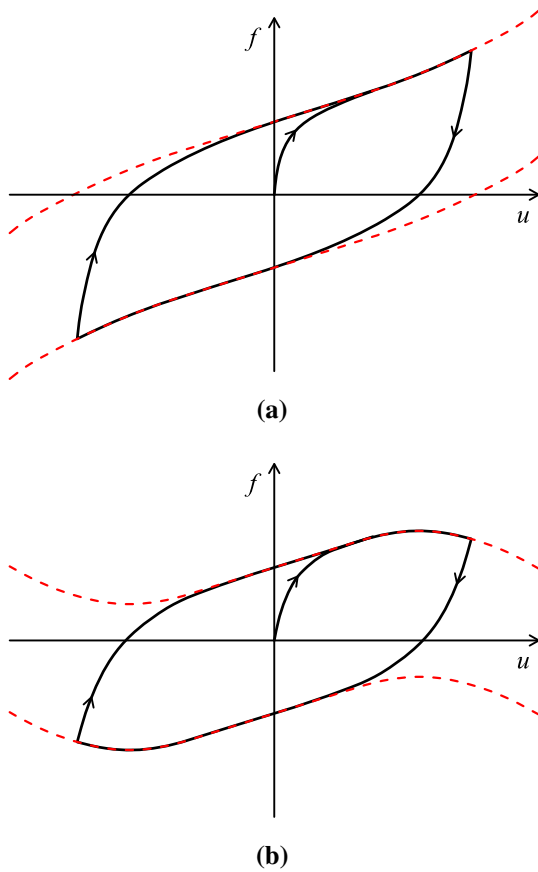


Fig. 2 An example of hysteresis loop limited by two curves typical of mechanical systems and materials exhibiting kinematic hardening (a) and softening (b) behavior

Hysteretic behavior characterized by hysteresis loops limited by two parallel straight lines is typical of many materials, such as ductile metals, e.g., steel [67], and geomaterials, e.g., soils [55] and concrete [4]. This hysteretic behavior is also typical of structural joints, such as steel [22], masonry [37], and wooden [52] joints, structural elements, e.g., steel braces [70], and seismic isolation bearings, such as wire rope isolators [60], steel dampers [30], and recycled rubber–fiber reinforced bearings [54].

Hysteretic behavior characterized by hysteresis loops limited by two parallel curves is typical of some structural joints [19], seismic devices, such as wire rope isolators [61], high damping rubber bearings [57], elastomeric seismic isolators [40], and recent hysteretic devices [9].

Generally, the above-described hysteretic behaviors are modeled in the literature [58, 59] using a uniax-

ial hysteretic spring parallel to a nonlinear elastic one, whose generalized tangent stiffnesses are k_h and k_e , respectively. The former allows one to reproduce hysteresis loops limited by two straight lines, whereas the latter allows one to modify the shape of the straight lines to obtain two parallel limiting curves. This basic idea is generalized in the following section by assigning suitably defined functional forms to k_h and k_e .

3 Proposed class of uniaxial phenomenological models

Mathematical modeling of hysteresis phenomena observed in mechanical systems and materials is very challenging, especially if the main aim is the development of accurate and computationally efficient models based on a small number of parameters having a clear mechanical significance.

In this section, a general formulation of a class of uniaxial phenomenological models, able to accurately simulate rate-independent mechanical hysteresis phenomena, is presented. More specifically, after some preliminaries about the adopted nomenclature, the proposed general form of the generalized tangent stiffness k_t , obtained by the sum of k_h and k_e , is described; subsequently, the general expressions for the generalized force f and for the history variable u_j are derived.

3.1 Preliminaries

Let c_u and c_l denote the upper and the lower limiting curves of a hysteresis loop, as shown in Fig. 3. The former intercepts the vertical axis at $f = \bar{f}$, whereas the latter at $f = -\bar{f}$. Assuming that cyclic loading phenomena do not modify the limiting curves, the distance between the two curves, along the vertical axis, is constant and equal to $2\bar{f}$.

Let c^+ denote the generic loading curve connecting points lying on the lower limiting curve c_l , having abscissa u_i^+ , with points on the upper limiting curve c_u , having abscissa u_j^+ , with $u_i^+ = u_j^+ - 2u_0$. Furthermore, let c^- denote the generic unloading curve connecting points lying on the upper limiting curve c_u , having abscissa u_i^- , with points on the lower limiting curve c_l , having abscissa u_j^- , with $u_i^- = u_j^- + 2u_0$. The $+$ ($-$) sign used as superscript is reminiscent of loading

(unloading) curves starting from the lower (upper) limiting curves. Furthermore, the subscript i (j) denotes the starting (ending) point of each curve.

The curves $c_u, c_l, c^+,$ and c^- , in the case of a hysteresis loop limited by two parallel straight lines (curves), are shown in Fig. 3a, b. Notice that, for simplicity, the loading (unloading) curves have been further specified by means of arrows directly plotted on the curves. More specifically, a loading (unloading) curve is the one characterized by a positive (negative) sign of the velocity.

3.2 Generalized tangent stiffness

In the proposed formulation, the generalized tangent stiffness k_t is given in the following general form:

$$k_t(u, u_j) = k_e(u) + k_h(u, u_j), \tag{1}$$

where $k_h(u, u_j)$ is a function of a relative generalized displacement, obtained by relating the absolute displacement u to the history variable u_j ; this last one is represented by u_j^+ , when $\dot{u} > 0$ (generic loading case), and by u_j^- , when $\dot{u} < 0$ (generic unloading case), where \dot{u} is the time derivative of the generalized displacement u .

As an example, assuming $k_e(u) = 0$, Fig. 4a, b shows the graph of the function $k_t(u, u_j)$ for the generic loading (unloading) curve c^+ (c^-) of Fig. 3a. In particular, the generalized tangent stiffness is a nonlinearly decreasing function, from k_a to k_b , on $[u_j^+ - 2u_0, u_j^+]$ when $\dot{u} > 0$, or on $[u_j^-, u_j^- + 2u_0]$ when $\dot{u} < 0$, being constant and equal to k_b on $[u_j^+, \infty)$ when $\dot{u} > 0$, or on $(-\infty, u_j^-]$ when $\dot{u} < 0$.

The choice of a more elaborate analytical function to describe the generalized tangent stiffness may require the selection of an increasing number of model parameters. Such parameters are obtained by calibrating the curves of the hysteresis loop on the basis of the results of experimental tests.

3.3 Generalized force

According to Fig. 3, in the generic loading case, it turns out to be $f = c^+$ when $u_i^+ < u < u_j^+$, and $f = c_u$ when $u > u_j^+$, whereas, in the generic unloading case, $f = c^-$ when $u_j^- < u < u_i^-$, and $f = c_l$ when

$u < u_j^-$. Thus, in the sequel, the expressions for the upper (c_u) and lower (c_l) limiting curves as well as for the generic loading (c^+) and unloading (c^-) curves are derived by integrating the generalized tangent stiffness k_t given by Eq. (1).

3.3.1 Upper limiting curve

The upper limiting curve c_u can be obtained by integrating Eq. (1) as follows:

$$c_u(u, u_j^+) = \int k_e(u)du + \int k_h(u, u_j^+) du + C_u. \tag{2}$$

Being interested in expressing the function c_u , we can assume that $u > u_j^+$ so that $k_h(u, u_j^+)$ is constant and equal to k_b . Hence, Eq. (2) becomes:

$$c_u(u) = f_e(u) + k_b u + C_u, \tag{3}$$

where

$$f_e(u) = \int k_e(u)du. \tag{4}$$

The integration constant C_u can be determined by imposing that the curve c_u intercepts the vertical axis at $f = \bar{f}$:

$$f_e(0) + C_u = \bar{f}, \tag{5}$$

from which, assuming $f_e(0) = 0$:

$$C_u = \bar{f}. \tag{6}$$

Thus, the general expression for the upper limiting curve is:

$$c_u(u) = f_e(u) + k_b u + \bar{f}. \tag{7}$$

3.3.2 Lower limiting curve

The lower limiting curve c_l can be obtained by integrating Eq. (1) as follows:

$$c_l(u, u_j^-) = \int k_e(u)du + \int k_h(u, u_j^-) du + C_l. \tag{8}$$

Fig. 3 Curves c_u , c_l , c^+ , and c^- in the case of a hysteresis loop limited by two parallel straight lines (a) or curves (b)

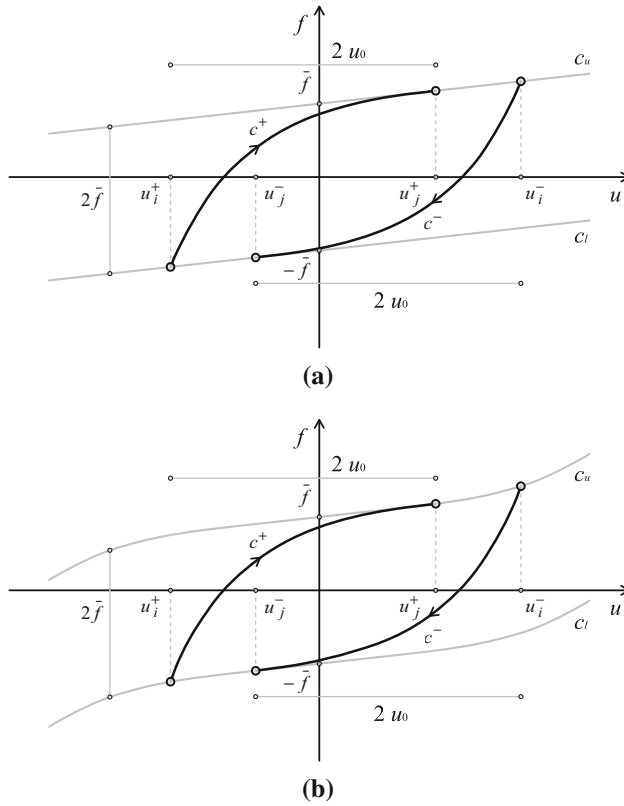
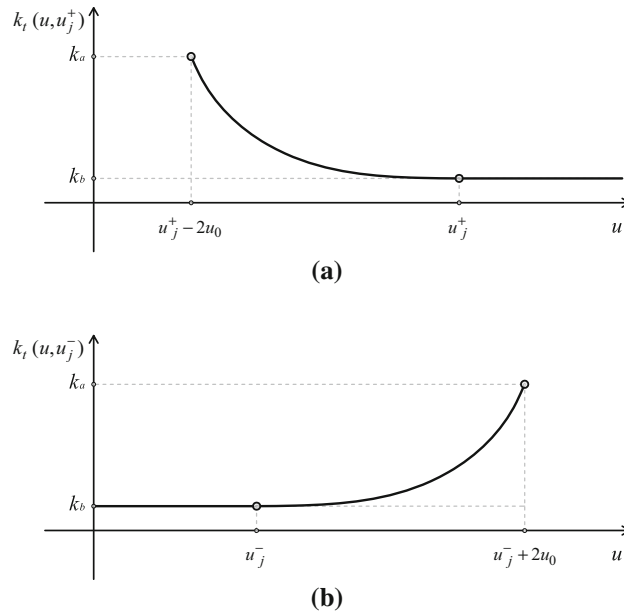


Fig. 4 Graph of function $k_l(u, u_j)$ for a generic loading (a) and unloading (b) case in Fig. 3a



As detailed for c_u , the function c_l comes into play when $u < u_j^-$, a condition for which $k_h(u, u_j^-)$ is constant and equal to k_b . Hence, Eq. (8) becomes:

$$c_l(u) = f_e(u) + k_b u + C_l, \tag{9}$$

where $f_e(u)$ is given by Eq. (4). The integration constant C_l can be determined by imposing that the curve c_l intercepts the vertical axis at $f = -\bar{f}$:

$$f_e(0) + C_l = -\bar{f}, \tag{10}$$

from which, assuming $f_e(0) = 0$, one infers:

$$C_l = -\bar{f}. \tag{11}$$

Thus, the general expression for the lower limiting curve is:

$$c_l(u) = f_e(u) + k_b u - \bar{f}. \tag{12}$$

It is apparent that the upper and lower limiting curves are parallel and that the distance between them, along the vertical axis, is equal to $2\bar{f}$.

3.3.3 Generic loading curve

The generic loading curve c^+ can be obtained by integrating Eq. (1) as follows:

$$c^+(u, u_j^+) = \int k_e(u) du + \int k_h(u, u_j^+) du + C^+, \tag{13}$$

or, equivalently

$$c^+(u, u_j^+) = f_e(u) + f_h(u, u_j^+) + C^+, \tag{14}$$

where $f_e(u)$ is given by Eq. (4), whereas $f_h(u, u_j^+)$ is evaluated as:

$$f_h(u, u_j^+) = \int k_h(u, u_j^+) du. \tag{15}$$

The integration constant C^+ can be determined by imposing that the generic loading curve c^+ intersects

the upper limiting curve c_u at $u = u_j^+$:

$$c^+(u_j^+, u_j^+) = c_u(u_j^+); \tag{16}$$

hence, on account of (7), one has:

$$f_e(u_j^+) + f_h(u_j^+, u_j^+) + C^+ = f_e(u_j^+) + k_b u_j^+ + \bar{f}, \tag{17}$$

from which one gets:

$$C^+ = k_b u_j^+ + \bar{f} - f_h(u_j^+, u_j^+). \tag{18}$$

In conclusion, the general expression for the generic loading curve is:

$$c^+(u, u_j^+) = f_e(u) + f_h(u, u_j^+) + k_b u_j^+ + \bar{f} - f_h(u_j^+, u_j^+). \tag{19}$$

To show that the model parameters \bar{f} and u_0 are related, we impose that the generic loading curve c^+ intersects the lower limiting curve at $u = u_i^+$. Thus, remembering that $u_i^+ = u_j^+ - 2u_0$ and setting:

$$c^+(u_j^+ - 2u_0, u_j^+) = c_l(u_j^+ - 2u_0), \tag{20}$$

the following equation is obtained, on account of (12):

$$f_e(u_j^+ - 2u_0) + f_h(u_j^+ - 2u_0, u_j^+) + k_b u_j^+ + \bar{f} - f_h(u_j^+, u_j^+) = f_e(u_j^+ - 2u_0) + k_b(u_j^+ - 2u_0) - \bar{f}, \tag{21}$$

and the general expression relating \bar{f} to u_0 is:

$$f_h(u_j^+ - 2u_0, u_j^+) + 2k_b u_0 + 2\bar{f} - f_h(u_j^+, u_j^+) = 0. \tag{22}$$

As shown in Sect. 4, Eq. (22) can be solved for \bar{f} or u_0 either in closed form or numerically depending on the type of function f_h obtained by integrating the selected generalized tangent stiffness function k_h .

3.3.4 Generic unloading curve

The generic unloading curve c^- can be obtained by integrating Eq. (1) as follows:

$$c^-(u, u_j^-) = \int k_e(u)du + \int k_h(u, u_j^-) du + C^-, \tag{23}$$

or, equivalently

$$c^-(u, u_j^-) = f_e(u) + f_h(u, u_j^-) + C^-, \tag{24}$$

where $f_e(u)$ is given by Eq. (4), whereas $f_h(u, u_j^-)$ is defined by:

$$f_h(u, u_j^-) = \int k_h(u, u_j^-) du. \tag{25}$$

The integration constant C^- can be determined by imposing that the generic unloading curve c^- intersects the lower limiting curve c_l at $u = u_j^-$:

$$c^-(u_j^-, u_j^-) = c_l(u_j^-); \tag{26}$$

hence, on account of (12), one has:

$$f_e(u_j^-) + f_h(u_j^-, u_j^-) + C^- = f_e(u_j^-) + k_b u_j^- - \bar{f}, \tag{27}$$

from which

$$C^- = k_b u_j^- - \bar{f} - f_h(u_j^-, u_j^-). \tag{28}$$

Thus, the general expression for the generic unloading curve is:

$$c^-(u, u_j^-) = f_e(u) + f_h(u, u_j^-) + k_b u_j^- - \bar{f} - f_h(u_j^-, u_j^-). \tag{29}$$

By imposing that the generic unloading curve c^- intersects the upper limiting curve at $u = u_i^-$, it is possible to derive a further general expression relating \bar{f} to u_0 . Thus, remembering that $u_i^- = u_j^- + 2u_0$ and setting:

$$c^-(u_j^- + 2u_0, u_j^-) = c_u(u_j^- + 2u_0), \tag{30}$$

the following equation is obtained on account of (7):

$$f_e(u_j^- + 2u_0) + f_h(u_j^- + 2u_0, u_j^-) + k_b u_j^- - \bar{f} - f_h(u_j^-, u_j^-) = f_e(u_j^- + 2u_0) + k_b(u_j^- + 2u_0) + \bar{f}. \tag{31}$$

In conclusion, the general expression relating \bar{f} to u_0 is:

$$f_h(u_j^- + 2u_0, u_j^-) - 2k_b u_0 - 2\bar{f} - f_h(u_j^-, u_j^-) = 0, \tag{32}$$

which complements the analogous relation (22).

3.4 History variable

Figure 5 shows a generic loading (unloading) curve having an initial point $P : (u_P, f_P)$ that lies between the two limiting curves. In this case, the distance, along the horizontal axis, required to reach the upper (lower) limiting curve, is equal to $u_j^+ - u_P$ ($|u_j^- - u_P|$) and, therefore, it is smaller than $2u_0$. The generalized displacement $u_j^+ (u_j^-)$, required to evaluate the generalized force f , has been previously presented as a history variable since it determines the current behavior of the system as a function of the previous states. However, we will show in the sequel that this variable can actually be computed for any starting point P ; hence, there is no reason for storing its value, as it happens for classical history variables, if not for the practical goal of enhancing the computational efficiency of the implementation.

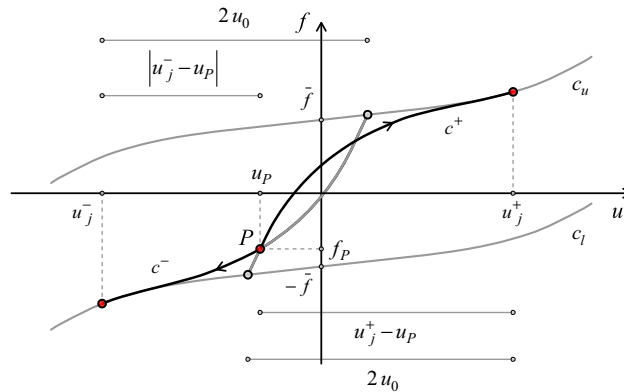
In the following, the general expressions for u_j^+ and u_j^- are derived for any starting point P .

3.4.1 Evaluation of u_j^+

The generic loading curve c^+ , shown in Fig. 5, is given by Eq. (19). By imposing that c^+ passes through the point $P : (u_P, f_P)$, the following equation is obtained:

$$c^+(u_P, u_j^+) = f_P, \tag{33}$$

Fig. 5 Evaluation of the history variable u_j



which gives

$$f_e(u_P) + f_h(u_P, u_j^+) + k_b u_j^+ + \bar{f} - f_h(u_j^+, u_j^+) = f_P, \tag{34}$$

from which u_j^+ can be evaluated.

3.4.2 Evaluation of u_j^-

The generic unloading curve c^- , shown in Fig. 5, is given by Eq. (29). By imposing that c^- passes through the point $P : (u_P, f_P)$, the following equation is obtained:

$$c^-(u_P, u_j^-) = f_P, \tag{35}$$

which gives

$$f_e(u_P) + f_h(u_P, u_j^-) + k_b u_j^- - \bar{f} - f_h(u_j^-, u_j^-) = f_P. \tag{36}$$

Both u_j^+ , by means of (34), and u_j^- , by means of the expression above, can be evaluated in closed form or numerically depending on the type of function f_h obtained by integrating the selected generalized tangent stiffness function k_h . This will be addressed in the next section considering two hysteretic models.

4 Two instances of the presented class: the Bilinear and Exponential Models

In this section, two hysteretic models, namely Bilinear Model (BM) and Exponential Model (EM) that repre-

sent two specific instances of the proposed class are developed by using the general formulation described in Sect. 3.

The Bilinear Model, able to simulate hysteresis loops limited by two parallel straight lines, is one of the simplest hysteretic models that can be emanated from the presented class; thus, it is described to easily illustrate the meaning of the adopted quantities.

The Exponential Model, able to simulate the hysteresis loops limited by two parallel straight lines or curves, is presented to show the potentialities of the proposed class, since it can be adopted to accurately simulate more complex rate-independent hysteretic behaviors.

By selecting general tangent stiffness functions different from the ones adopted in the Bilinear and Exponential Models and by applying the general relations of Sect. 3, it is possible to derive new models characterized by hysteretic loops of different shapes and by different computational features in terms of numerical accuracy and efficiency.

4.1 Bilinear Model

4.1.1 Generalized tangent stiffness

The selected generalized tangent stiffness functions are:

$$k_e(u) = 0 \quad \text{on } (-\infty, \infty), \tag{37}$$

$$k_h(u, u_j^+) = \begin{cases} k_a & \text{on } [u_j^+ - 2u_0, u_j^+] \\ k_b & \text{on }]u_j^+, \infty) \end{cases} \tag{38a}$$

$$k_h(u, u_j^-) = \begin{cases} k_a & \text{on }]u_j^-, u_j^- + 2u_0] \\ k_b & \text{on } (-\infty, u_j^-[. \end{cases} \quad (39a)$$

$$(39b)$$

Thus, the model parameters to be calibrated from experimental tests are k_a, k_b , and u_0 . We further assume that $k_a > k_b, k_a > 0$, and that $u_0 > 0$.

Notice that the function k_h is discontinuous at u_j^+ (u_j^-). This is due to the different value assumed by the tangents at u_j^+ for the two curves c^+ and c_u . The same property does hold at u_j^- if one considers the curves c^- and c_l . The graph of the function k_h is plotted in Fig. 6 for the generic loading case.

4.1.2 Generalized force

The expressions for the upper (lower) limiting curve c_u (c_l) and for the generic loading (unloading) curve c^+ (c^-) are first derived; subsequently, the expression for \bar{f} , required for the evaluation of c_u, c_l, c^+ , and c^- , is obtained.

Upper (lower) limiting curve

According to the definition (4) and to the assumption (37), it turns out to be:

$$f_e(u) = 0. \quad (40)$$

Hence, Eq. (7) yields:

$$c_u(u) = k_b u + \bar{f}, \quad (41)$$

whereas Eq. (12) becomes:

$$c_l(u) = k_b u - \bar{f}. \quad (42)$$

Generic loading (unloading) curve

On account of the assumption (38a), Eq. (15) specializes to:

$$f_h(u, u_j^+) = k_a u, \quad (43)$$

so that Eq. (19) yields:

$$c^+(u, u_j^+) = k_a(u - u_j^+) + k_b u_j^+ + \bar{f}. \quad (44)$$

Similarly, because of the assumption (39a), Eq. (25) becomes:

$$f_h(u, u_j^-) = k_a u. \quad (45)$$

Hence, Eq. (29) yields:

$$c^-(u, u_j^-) = k_a(u - u_j^-) + k_b u_j^- - \bar{f}. \quad (46)$$

Expression for \bar{f}

The expression for \bar{f} can be obtained by using Eqs. (22) and (43) to get:

$$k_a(u_j^+ - 2u_0) + 2k_b u_0 + 2\bar{f} - k_a u_j^+ = 0, \quad (47)$$

from which we obtain:

$$\bar{f} = (k_a - k_b)u_0, \quad (48)$$

an expression providing a positive value of \bar{f} . The same result is arrived at by exploiting Eq. (32).

4.1.3 History variable

Involving (40) and (43), Eq. (34) specializes to:

$$k_a u_P + k_b u_j^+ + \bar{f} - k_a u_j^+ = f_P, \quad (49)$$

from which the following expression of the history variable, holding for the loading case, is obtained:

$$u_j^+ = \frac{k_a u_P + \bar{f} - f_P}{k_a - k_b}. \quad (50)$$

Similarly, using (40) and (45), Eq. (36) becomes:

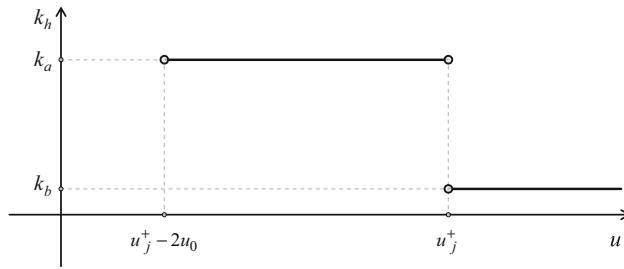
$$k_a u_P + k_b u_j^- - \bar{f} - k_a u_j^- = f_P, \quad (51)$$

from which the following expression of the history variable, holding for the unloading case, is obtained:

$$u_j^- = \frac{k_a u_P - \bar{f} - f_P}{k_a - k_b}. \quad (52)$$

Note that the history variable u_j^+ (u_j^-) may be positive or negative according to the coordinates of the initial point P of the generic loading (unloading) curve.

Fig. 6 Graph of function k_h for the generic loading case (Bilinear Model)



4.1.4 Hysteresis loop shape

Figure 7 shows two different shapes of the generalized force–displacement hysteresis loop obtained by applying a sinusoidal generalized displacement of unit amplitude and simulated by adopting the Bilinear Model parameters listed in Table 1. More specifically, Fig. 7a, b shows a hysteresis loop bounded by two straight lines typical of kinematic hardening (softening) mechanical systems and materials. Note that, although the hysteresis loop of Fig. 7b does not simulate a realistic softening behavior, it has been plotted to illustrate the properties of the Bilinear Model.

4.2 Exponential Model

4.2.1 Generalized tangent stiffness

The selected generalized tangent stiffness functions are:

$$k_e(u) = -2\beta + \beta (e^{\beta u} + e^{-\beta u}) \quad \text{on } (-\infty, \infty), \tag{53}$$

$$k_h(u, u_j^+) = \begin{cases} k_b + (k_a - k_b)e^{-\alpha(u - u_j^+ + 2u_0)} & \text{on } [u_j^+ - 2u_0, u_j^+] \\ k_b & \text{on }]u_j^+, \infty[\end{cases} \tag{54a}$$

$$\tag{54b}$$

$$k_h(u, u_j^-) = \begin{cases} k_b + (k_a - k_b)e^{-\alpha(-u + u_j^- + 2u_0)} & \text{on }]u_j^-, u_j^- + 2u_0] \\ k_b & \text{on } (-\infty, u_j^-[\end{cases} \tag{55a}$$

$$\tag{55b}$$

where $k_a > k_b$, $k_a > 0$, $u_0 > 0$, $\alpha > 0$, and β is real. They represent the model parameters to be calibrated

from experimental tests. In particular, the parameter β defines the shape of function k_e , a function that is convex on $(-\infty, \infty)$, when $\beta > 0$, whereas it is concave on $(-\infty, \infty)$, when $\beta < 0$.

Function k_h is a nonlinearly decreasing function, from k_a to $k_b + (k_a - k_b)e^{-2\alpha u_0}$, on $[u_j^+ - 2u_0, u_j^+]$, when $\dot{u} > 0$, and on $]u_j^-, u_j^- + 2u_0]$, when $\dot{u} < 0$; moreover, k_h is equal to k_b on $]u_j^+, \infty)$, when $\dot{u} > 0$, and on $(-\infty, u_j^-]$, when $\dot{u} < 0$. The positive parameter α rules the rate of variation of k_h from k_a to $k_b + (k_a - k_b)e^{-2\alpha u_0}$. Figure 8 shows the graph of the function k_h for the generic loading case.

Note that the function k_h is discontinuous at u_j^\pm (u_j^\pm). Denoting by δ_k the difference between the two different stiffness values at u_j^\pm (u_j^\pm), as shown in Fig. 8 for the generic loading case, we can write:

$$(k_a - k_b)e^{-2\alpha u_0} = \delta_k, \tag{56}$$

from which we obtain:

$$u_0 = -\frac{1}{2\alpha} \ln \left(\frac{\delta_k}{k_a - k_b} \right), \tag{57}$$

an expression yielding positive values of u_0 for $\delta_k > 0$. To have a generic loading (unloading) curve c^+ (c^-) that smoothly approaches the upper (lower) limiting curve c_u (c_l), i.e., with a generalized tangent stiffness at u_j^\pm (u_j^\pm) very close to the one of the upper (lower) limiting curve c_u (c_l), one should set $\delta_k = 0$ in (57), thus making u_0 undefined. However, the extensive numerical tests which have been carried out, only partially documented in the next section, have proved that a value $\delta_k = 10^{-20}$ suffices for practical purposes.

4.2.2 Generalized force

After deriving the expressions for the upper (lower) limiting curve c_u (c_l) and for the generic loading

Fig. 7 Hysteresis loops simulated by adopting the Bilinear Model parameters given in Table 1

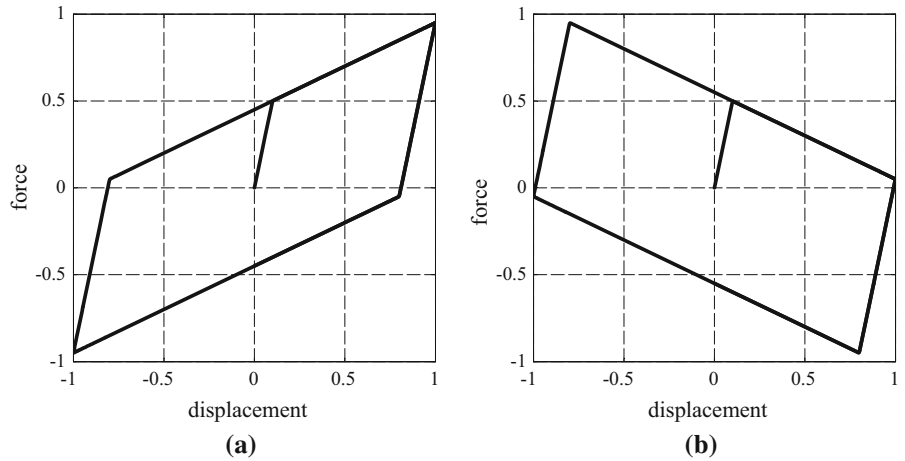
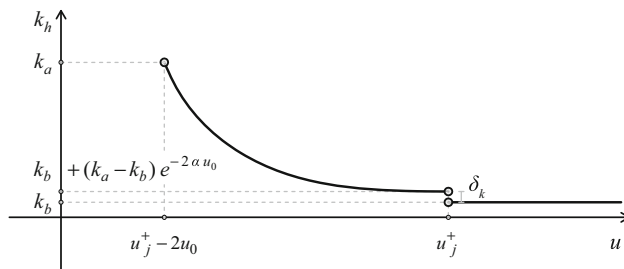


Table 1 Bilinear Model parameters

	k_a	k_b	u_0
(a)	5.0	0.5	0.1
(b)	5.0	-0.5	4.7

Fig. 8 Graph of function k_h for the generic loading case (Exponential Model)



(unloading) curve c^+ (c^-), we obtain the expression for \bar{f} required for the evaluation of c_u , c_l , c^+ , and c^- .

Upper (lower) limiting curve

According to the definition (4) and to the assumption (53), it turns out to be:

$$f_e(u) = -2\beta u + e^{\beta u} - e^{-\beta u}. \tag{58}$$

Hence, Eq. (7) yields:

$$c_u(u) = -2\beta u + e^{\beta u} - e^{-\beta u} + k_b u + \bar{f}, \tag{59}$$

whereas Eq. (12) becomes:

$$c_l(u) = -2\beta u + e^{\beta u} - e^{-\beta u} + k_b u - \bar{f}. \tag{60}$$

Generic loading (unloading) curve

On account of the assumption (54a), Eq. (15) specializes to:

$$f_h(u, u_j^+) = k_b u - \frac{(k_a - k_b)}{\alpha} e^{-\alpha(u - u_j^+ + 2u_0)}, \tag{61}$$

so that, recalling (58), Eq. (19) yields:

$$c^+(u, u_j^+) = -2\beta u + e^{\beta u} - e^{-\beta u} + k_b u - \frac{(k_a - k_b)}{\alpha} \left[e^{-\alpha(u - u_j^+ + 2u_0)} - e^{-2\alpha u_0} \right] + \bar{f}. \tag{62}$$

Similarly, because of the assumption (55a), Eq. (25) becomes:

$$f_h(u, u_j^-) = k_b u + \frac{(k_a - k_b)}{\alpha} e^{-\alpha(-u+u_j^-+2u_0)}. \tag{63}$$

Substituting the previous expression in Eq. (29) and recalling (58), one obtains:

$$c^-(u, u_j^-) = -2\beta u + e^{\beta u} - e^{-\beta u} + k_b u + \frac{(k_a - k_b)}{\alpha} \left[e^{-\alpha(-u+u_j^-+2u_0)} - e^{-2\alpha u_0} \right] - \bar{f}. \tag{64}$$

Expression for \bar{f}

The expression for \bar{f} can be obtained by using Eq. (22) or (32). Adopting (61), the former equation becomes:

$$k_b(u_j^+ - 2u_0) - \frac{(k_a - k_b)}{\alpha} + 2k_b u_0 + 2\bar{f} - k_b u_j^+ + \frac{(k_a - k_b)}{\alpha} e^{-2\alpha u_0} = 0, \tag{65}$$

from which we obtain:

$$\bar{f} = \frac{(k_a - k_b)}{2\alpha} (1 - e^{-2\alpha u_0}). \tag{66}$$

Since $\alpha > 0$ and $u_0 > 0$, the previous expression provides a positive value of \bar{f} .

4.2.3 History variable

Involving (58) and (61), Eq. (34) specializes to:

$$-2\beta u_P + e^{\beta u_P} - e^{-\beta u_P} + k_b u_P - \frac{(k_a - k_b)}{\alpha} e^{-\alpha(u_P - u_j^+ + 2u_0)} + k_b u_j^+ + \bar{f} - k_b u_j^+ + \frac{(k_a - k_b)}{\alpha} e^{-2\alpha u_0} = f_P, \tag{67}$$

from which the following expression of the history variable, holding for the loading case, is obtained:

$$u_j^+ = u_P + 2u_0 + \frac{1}{\alpha} \ln \left[\frac{\alpha}{(k_a - k_b)} (-2\beta u_P + e^{\beta u_P} - e^{-\beta u_P} + k_b u_P + \frac{(k_a - k_b)}{\alpha} e^{-2\alpha u_0} + \bar{f} - f_P) \right]. \tag{68}$$

Similarly, using (58) and (63), Eq. (36) becomes:

$$-2\beta u_P + e^{\beta u_P} - e^{-\beta u_P} + k_b u_P + \frac{(k_a - k_b)}{\alpha} e^{-\alpha(-u_P + u_j^- + 2u_0)} + k_b u_j^- - \bar{f} - k_b u_j^- - \frac{(k_a - k_b)}{\alpha} e^{-2\alpha u_0} = f_P, \tag{69}$$

from which the following expression of the history variable, valid for the unloading case, is obtained:

$$u_j^- = u_P - 2u_0 - \frac{1}{\alpha} \ln \left[-\frac{\alpha}{(k_a - k_b)} (-2\beta u_P + e^{\beta u_P} - e^{-\beta u_P} + k_b u_P - \frac{(k_a - k_b)}{\alpha} e^{-2\alpha u_0} - \bar{f} - f_P) \right]. \tag{70}$$

The history variable u_j^+ (u_j^-) may be positive or negative according to the coordinates of the initial point P of the generic loading (unloading) curve. In any case, the argument of the logarithm in Eqs. (68) and (70) is positive if $k_a > k_b$, $k_a > 0$, $u_0 > 0$, and $\alpha > 0$. To show this, we consider the argument of the logarithm in Eq. (68):

$$\arg = \frac{\alpha}{(k_a - k_b)} (-2\beta u_P + e^{\beta u_P} - e^{-\beta u_P} + k_b u_P + \frac{(k_a - k_b)}{\alpha} e^{-2\alpha u_0} + \bar{f} - f_P), \tag{71}$$

and we show that its minimum value \arg_{\min} is always positive. Making reference to Fig. 5, we remember that u_j^+ has two extreme values, which are $u_P + 2u_0$, when P lies on the lower limiting curve c_l , and u_P , when P

lies on the upper limiting curve c_u ; hence, the argument of the logarithm in (68) has to be equal to 1 in the former case and equal to $\frac{\delta_k}{k_a - k_b}$ in the latter. Since $\delta_k = 10^{-20} \ll 1$, we have:

$$\arg_{\min} = \frac{\delta_k}{k_a - k_b}, \tag{72}$$

a quantity that is always positive.

4.2.4 Hysteresis loop shape

Figure 9 shows four different shapes of the generalized force–displacement hysteresis loop obtained by applying a sinusoidal generalized displacement of unit amplitude and simulated by adopting the Exponential Model parameters listed in Table 2. More specifically, Fig. 9a, c shows a hysteresis loop bounded by two straight lines (curves) typical of kinematic hardening mechanical systems and materials, whereas the hysteresis loop diagrammed in Fig. 9b, d is typical of kinematic softening behaviors. Note that, although the hysteresis loop of Fig. 9b does not simulate a realistic softening behavior, it has been plotted to illustrate the properties of the Exponential Model.

Figure 10 illustrates the influence of each EM parameter on the size and/or shape of hysteresis loops produced by imposing a sinusoidal generalized unit displacement. More specifically, the hysteresis loops in Fig. 10a have been obtained adopting $k_b = 0.5$, $\alpha = 5$, $\beta = 0$, and three different values of k_a , that is 5, 10, and 15. It is evident that the increase of k_a produces an increase of the size of the hysteresis loop without modifying its shape.

Figure 10b, c shows hysteresis loops simulated using $k_a = 5$, $\alpha = 5$, $\beta = 0$, and three values of k_b , that is, 0, 0.5, and 1 (0, -0.5 , and -1). It can be observed that the increase (decrease) of k_b produces a counterclockwise (clockwise) rotation of the hysteresis loop and a slight decrease (increase) of its size.

The hysteresis loops in Fig. 10d have been obtained setting $k_a = 5$, $k_b = 0.5$, $\beta = 0$, and adopting three different values of α , that is, 5, 10, and 15. This figure reveals that the increase of α allows the reduction of the hysteresis loop size without modifying its shape.

Finally, Fig. 10e, f presents hysteresis loops simulated using $k_a = 5$, $k_b = 0.5$, $\alpha = 5$, and three positive (negative) values of β , that is, 0, 1, and 1.5 (0, -1 , and

-1.5). It is evident that the parameter β significantly affects the hysteresis loop shape.

4.3 Computer implementation

For the reader’s convenience, a schematic flowchart of the Bilinear (Exponential) Model is presented in Tables 3 and 4. To this end, we suppose that a rate-independent mechanical system or material is subjected to a given time-dependent load and that a displacement-driven solution scheme has been adopted; hence, the generalized displacement history, in particular $u_{t-\Delta t}$ and u_t , is known over a time step Δt and the generalized force f_t has to be determined. Because of this assumption, the generalized velocity history, that is, $\dot{u}_{t-\Delta t}$ and \dot{u}_t , and the generalized force $f_{t-\Delta t}$ are also known.

Tables 3 and 4 summarize the implementation scheme for the Bilinear (Exponential) Model. The algorithm is composed of two parts. In the first one, called *Initial settings*, the model parameters are assigned and the associated internal ones are calculated. In the second one, called *Calculations at each time step*, the history variable u_j^+ (u_j^-) is updated if the sign of generalized velocity at time t , namely $s_t = \text{sgn}(\dot{u}_t)$, changes with respect to the one at $t - \Delta t$; then, the generalized force f_t is evaluated by adopting the expression of the generic loading (unloading) curve c^+ (c^-) if $u_j^+ - 2u_0 < u_t < u_j^+$ ($u_j^- < u_t < u_j^- + 2u_0$); otherwise it is evaluated by using the expression of the upper (lower) limiting curve c_u (c_l).

5 Numerical applications

In this section, the nonlinear dynamic response of a rate-independent kinematic hardening single degree of freedom mechanical system is simulated by modeling the generalized force of the system on the basis of the Exponential Model (EM) described in Sect. 4.

To demonstrate the accuracy of the EM and its capability to significantly decrease the computational burden of nonlinear time history analyses, the numerical results and the computational times are compared with those obtained by modeling the generalized force of the mechanical system with the Bouc–Wen Model (BWM) [8,65,66], which is one of the most used differential models in the literature [2,3,17,25,33,36,44]. Two dif-

Fig. 9 Hysteresis loops simulated by adopting the Exponential Model parameters given in Table 2

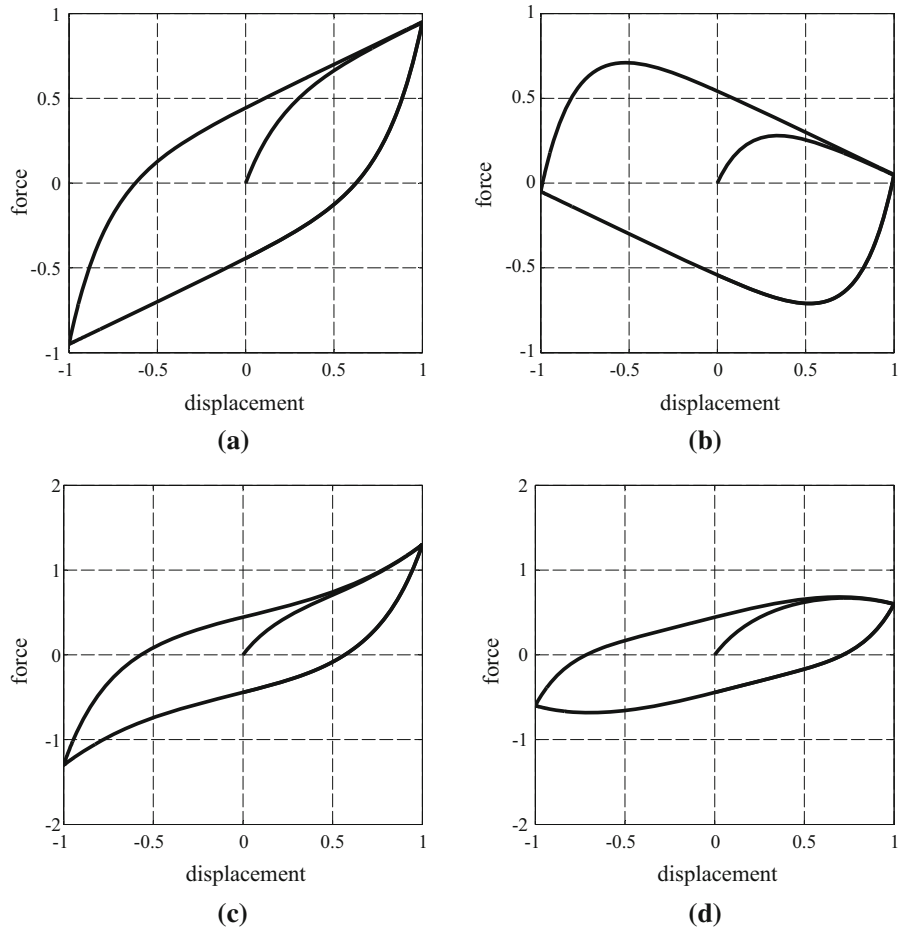


Table 2 Exponential Model parameters

	k_a	k_b	α	β
(a)	5.0	0.5	5.0	0.0
(b)	5.0	-0.5	5.0	0.0
(c)	5.0	0.5	5.0	1.0
(d)	5.0	0.5	5.0	-1.0

ferent external forces, that is, a harmonic and a random force, are considered in the analysis.

5.1 Analyzed mechanical system

We first consider a nonlinear mechanical system characterized by a single degree of freedom; its motion is described by the equation:

$$m\ddot{u} + f_d(\dot{u}) + f(u) = p(t), \tag{73}$$

where m denotes the mass of the system, u the generalized displacement, \dot{u} the generalized velocity, \ddot{u} the generalized acceleration, $f_d(\dot{u})$ the generalized rate-dependent force, $f(u)$ the generalized rate-independent force, and p the generalized external force depending upon time t . In rate-independent mechanical systems, the nonlinear ordinary differential equation given by Eq. (73) simplifies to:

$$m\ddot{u} + f(u) = p(t). \tag{74}$$

Fig. 10 Influence of the EM parameters on the size and/or shape of the hysteresis loops

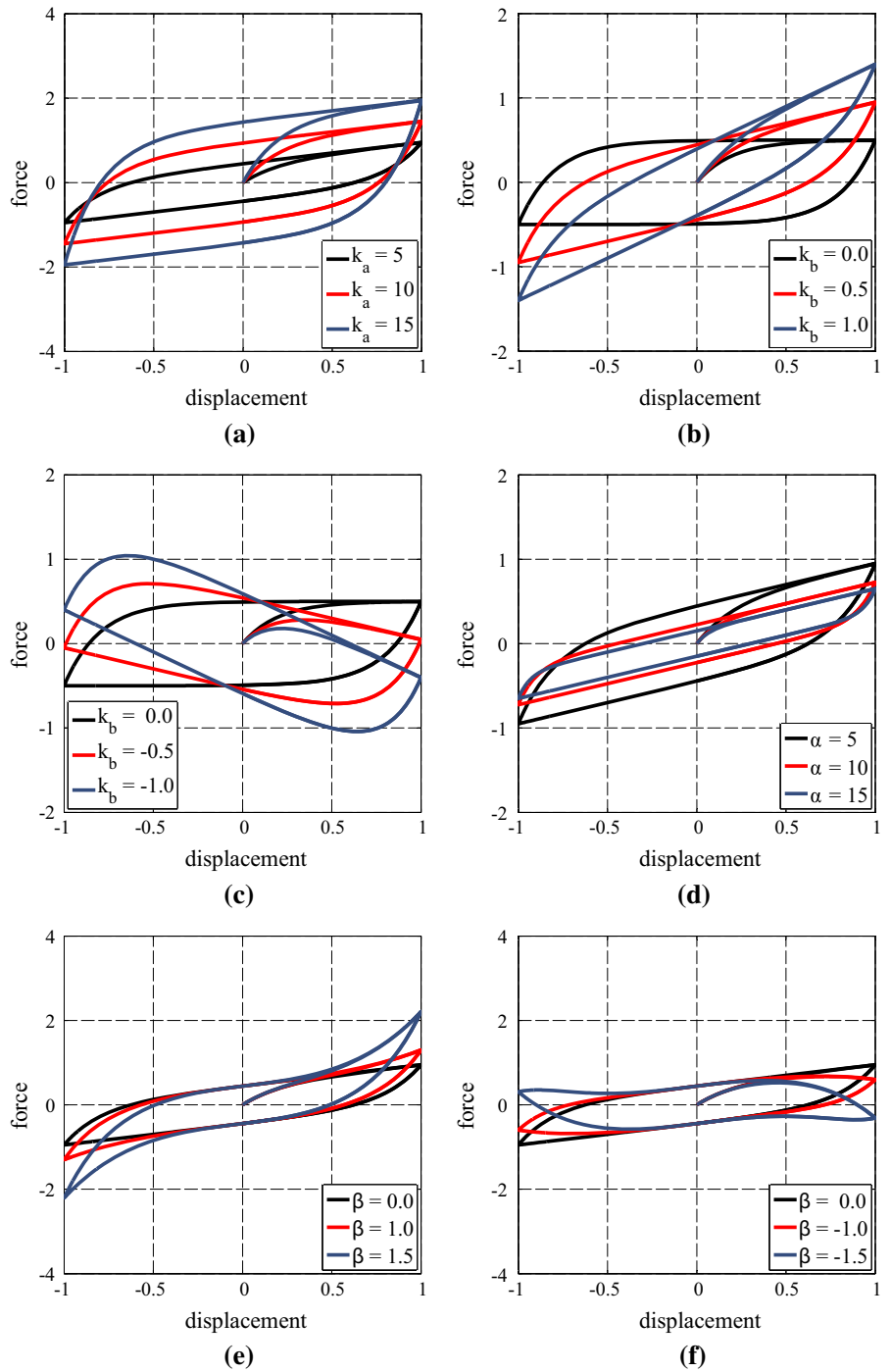


Table 3 Bilinear Model algorithm

1. Initial settings	
1.1	Set the three model parameters: k_a , k_b , and u_0
1.2	Compute the internal model parameter [see (48)]: $\bar{f} = (k_a - k_b)u_0$
2. Calculations at each time step	
2.1	If $s_t s_{t-\Delta t} < 0$, update the history variable [see (50) and (52)] $u_j = \frac{k_a u_{t-\Delta t} + \bar{f} s_t - f_{t-\Delta t}}{k_a - k_b}$
2.2	Evaluate the generalized force at time t if $u_j s_t - 2u_0 < u_t s_t < u_j s_t$ $f_t = k_a(u_t - u_j) + k_b u_j + \bar{f} s_t$ [see (44) and (46)] otherwise $f_t = k_b u_t + \bar{f} s_t$ [see (41) and (42)]

Table 4 Exponential Model algorithm

1. Initial settings	
1.1	Set the four model parameters: k_a , k_b , α , and β
1.2	Compute the internal model parameters [see (57) and (66)] $u_0 = -\frac{1}{2\alpha} \ln\left(\frac{\delta_k}{k_a - k_b}\right)$ and $\bar{f} = \frac{k_a - k_b}{2\alpha} (1 - e^{-2\alpha u_0})$, with $\delta_k = 10^{-20}$
2. Calculations at each time step	
2.1	If $s_t s_{t-\Delta t} < 0$, update the history variable [see (68) and (70)] $u_j = u_{t-\Delta t} + 2u_0 s_t + \frac{s_t}{\alpha} \ln\left[\frac{\alpha s_t}{k_a - k_b} \left(-2\beta u_{t-\Delta t} + e^{\beta u_{t-\Delta t}} - e^{-\beta u_{t-\Delta t}} + k_b u_{t-\Delta t} + \frac{k_a - k_b}{\alpha} s_t e^{-2\alpha u_0} + \bar{f} s_t - f_{t-\Delta t}\right)\right]$
2.2	Evaluate the generalized force at time t if $u_j s_t - 2u_0 < u_t s_t < u_j s_t$ $f_t = -2\beta u_t + e^{\beta u_t} - e^{-\beta u_t} + k_b u_t - s_t \frac{k_a - k_b}{\alpha} \left[e^{-\alpha(u_t s_t - u_j s_t + 2u_0)} - e^{-2\alpha u_0}\right] + \bar{f} s_t$ [see (62) and (64)] otherwise $f_t = -2\beta u_t + e^{\beta u_t} - e^{-\beta u_t} + k_b u_t + \bar{f} s_t$ [see (59) and (60)]

The properties of the analyzed rate-independent kinematic hardening mechanical system are listed in Table 5, where k_{ti} is the generalized pre-yield tangent stiffness, whereas k_{ty} is the constant value assumed by the generalized post-yield tangent stiffness for generalized displacements greater than $2u_y$.

5.2 Applied generalized external forces

The nonlinear dynamic response of the rate-independent mechanical system is simulated for two different external generalized forces: a harmonic force and a random force.

The harmonic force, shown in Fig. 11a, is a sinusoidal force having an amplitude p_0 that increases linearly with time from 0 to 5 N, forcing frequency $\omega_p = 2$ rad/s, and time duration $t_d = 10$ s.

The random force, shown in Fig. 11b, is a Gaussian white noise having intensity $i_{wn} = 7.5$ N, and time duration $t_d = 30$ s.

5.3 Model parameters

The generalized force in (74), simulating a large variety of hysteretic behaviors, is usually assigned by means of the celebrated Bouc–Wen Model, a so-called differential model based on the Duhem hysteresis operator [18].

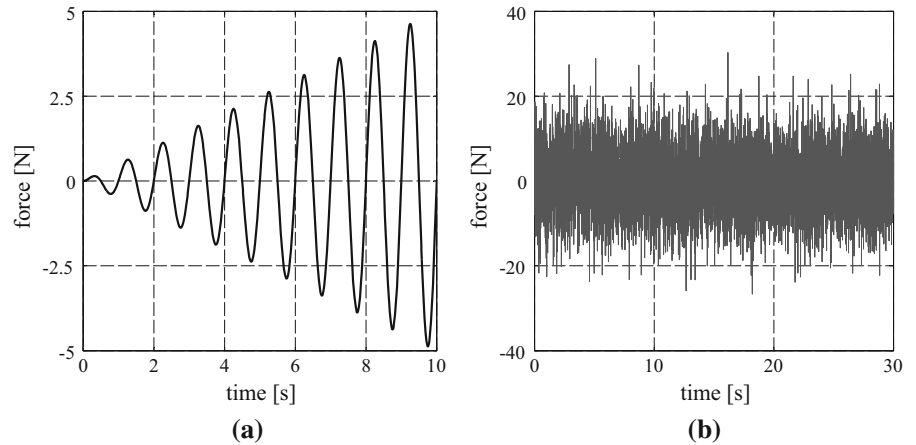
In particular, according to the Bouc–Wen Model, the generalized force of a mechanical system is given by:

$$f(u) = aku + (1 - a)kz, \tag{75}$$

Table 5 Analyzed mechanical system properties

m (Ns ² m ⁻¹)	k_{ii} (Nm ⁻¹)	k_{iy} (Nm ⁻¹)	u_y (m)
1	$32 \pi^2$	π^2	0.126

Fig. 11 Applied generalized external forces: **a** harmonic and **b** random force



where a is a dimensionless parameter, and k and d are parameters having dimension of stiffness and displacement, respectively. Finally, the adimensional variable z is obtained by solving the following first-order nonlinear ordinary differential equation:

$$\dot{z} = d^{-1} \left(A\dot{u} - b|\dot{u}|z|z|^{n-1} - c\dot{u}|z|^n \right), \tag{76}$$

where $A, b, c,$ and n are dimensionless parameters that control the hysteresis loop shape.

To simulate the nonlinear behavior of the analyzed mechanical system and to compare the computational features of the EM with the ones of the classical BWM, the parameters listed in Tables 6 and 7 have been adopted.

In the Exponential Model, the parameter β has been set equal to 0 to have two limiting straight lines; thus, being $k_e = 0, k_a = k_{ii}$ and $k_b = k_{iy}$. The parameter α has been evaluated adopting (57) with $u_0 = u_y$ and $\delta_k = 10^{-20}$.

In the Bouc–Wen Model, the following parameters $n = 1.5, A = 1, b = 1,$ and $c = 0$ have been used to obtain the desired hysteresis loop shape [28,59]. Furthermore, the parameters $k, a,$ and d have been selected so as to reproduce the hysteresis loops simulated with the Exponential Model.

A comparison between Tables 6 and 7 clearly shows that the EM requires a reduced number of parameters with respect to the celebrated BWM.

In addition, it has to be noted that an important benefit of the EM consists in the accurate determination of its parameters through an analytical fitting of the experimental hysteresis loops. Indeed, as it has been shown in 4.2.4, the EM parameters are directly associated with the graphical properties of the hysteresis loop. If more accurate identifications are required, usually of nonlinear nature, such computed parameters represent suitable first trial values for the iterations required to compute the *optimal* parameters, i.e., the ones that best fit the experimental curves according to the adopted criterion. Moreover, the peculiar analytical formulation of the proposed class permits a closed form computation of the response gradient, an issue of the outmost importance in identification procedures.

On the contrary, the interpretation of the BWM parameters is not straightforward and their identification from experimental data still remains an open issue which has been investigated over years by several approaches, depending on the peculiar formulation of the BWM [10,12,51,69].

Table 6 EM parameters adopted in numerical simulations

k_a (Nm ⁻¹)	k_b (Nm ⁻¹)	α	β
$32 \pi^2$	π^2	205	0

Table 7 BWM parameters adopted in numerical simulations

k (Nm ⁻¹)	a	d (m)	n	A	b	c
$16 \pi^2$	1/16	0.005	1.5	1	1	0

5.4 Results of the nonlinear time history analyses

In the sequel, the accuracy and the computational efficiency of the Exponential Model are assessed by presenting the results of some numerical simulations.

The equation of motion, given by Eq. (74), has been numerically solved by adopting a conventional solution approach, that is the explicit time integration central difference method [5, 24], and using a time step of 0.005 s. Furthermore, in the Bouc–Wen Model, the first-order nonlinear ordinary differential equation, given by Eq. (76), has been numerically solved by using the unconditionally stable semi-implicit Runge–Kutta method [50] and considering 50 steps. The solution algorithm and the hysteretic models have been programmed in MATLAB and run on a computer equipped with an Intel®Core™ i7-4700MQ processor and a CPU at 2.40 GHz with 16 GB of RAM.

The results of the nonlinear time history analyses (NLTHAs), associated with harmonic and random forces, are shown in Tables 8 and 9, respectively.

The accuracy of the EM is very satisfactory since the maximum and minimum values of the generalized displacements, velocities, and accelerations are numerically quite close to those predicted by the BWM.

However, the computational burden of the EM, expressed by the total computational time t_{ct} , is significantly reduced with respect to that characterizing the BWM. Clearly, the parameter t_{ct} is not a fully objective measure of the algorithmic efficiency, since it depends upon the amount of the background process running on the computer, the relevant memory and CPU speed; for this reason, t_{ct} has been normalized as:

$$EM\ tctp\ [\%] = \frac{EM\ t_{ct}}{BWM\ t_{ct}} \cdot 100, \tag{77}$$

to get a more meaningful measure of the computational benefits associated with the use of the EM with respect to the BWM.

Time histories of the mechanical system are illustrated in terms of generalized displacement, e.g., Fig. 12, generalized velocity, e.g., Fig. 13, and generalized acceleration, e.g., Fig. 14; generalized force–displacement hysteresis loops are shown in Fig. 15. Generally speaking, the comparison between the responses associated with the EM and the BWM shows a very good agreement.

6 Conclusions

We have presented a general formulation of a class of uniaxial phenomenological models, able to simulate hysteresis loops limited by two parallel straight lines or curves, typical of rate-independent mechanical systems and materials with kinematic hardening or softening hysteretic behavior. The proposed class of models requires only one history variable and leads to the solution of a scalar equation for the evaluation of the generalized force.

To illustrate the peculiar features of the proposed general formulation, two specific instances of the class, denominated Bilinear Model and Exponential Model, have been described. The Bilinear Model, able to simulate hysteresis loops limited by two parallel straight lines, is one of simplest models that can be emanated from the proposed class, whereas the Exponential Model, able to reproduce hysteresis loops limited by two parallel straight lines or curves, is a more elaborate model that can simulate the behavior of a wider spectrum of mechanical systems and materials.

To investigate the overall computational features of the EM, some nonlinear time history analyses have

Table 8 NLTHAs results | Harmonic force

	tct (s)	tctp	u (m)		\dot{u} (ms ⁻¹)		\ddot{u} (ms ⁻²)	
			max	min	max	min	max	min
BWM	8.98	–	0.1691	–0.1605	1.0210	–1.0734	6.8034	–7.1500
EM	0.06	0.66%	0.1690	–0.1604	1.0205	–1.0730	6.8046	–7.1546

Table 9 NLTHAs results | Random force

	tct (s)	tctp	u (m)		\dot{u} (ms ⁻¹)		\ddot{u} (ms ⁻²)	
			max	min	max	min	max	min
BWM	26.76	–	0.1225	–0.1803	0.7156	–0.5657	30.171	–25.893
EM	0.185	0.69%	0.1234	–0.1803	0.7183	–0.5627	30.148	–25.895

Fig. 12 Generalized displacement time history obtained applying the **a** harmonic and **b** random force

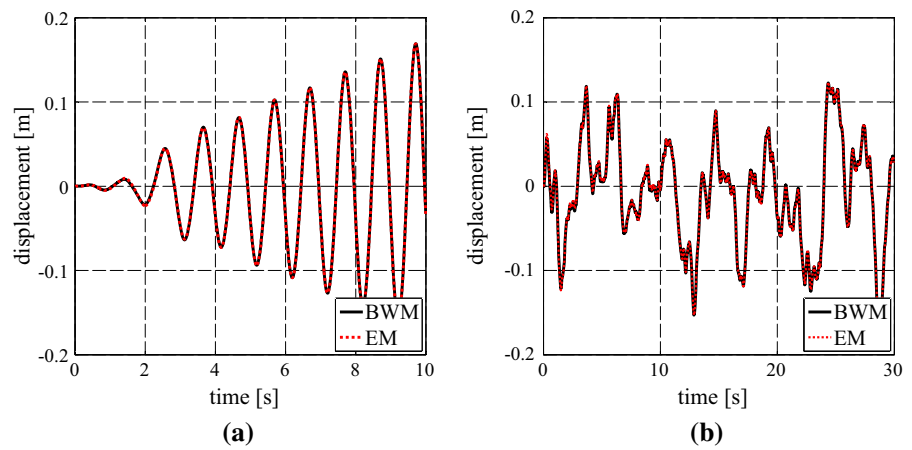


Fig. 13 Generalized velocity time history obtained applying the **a** harmonic and **b** random force

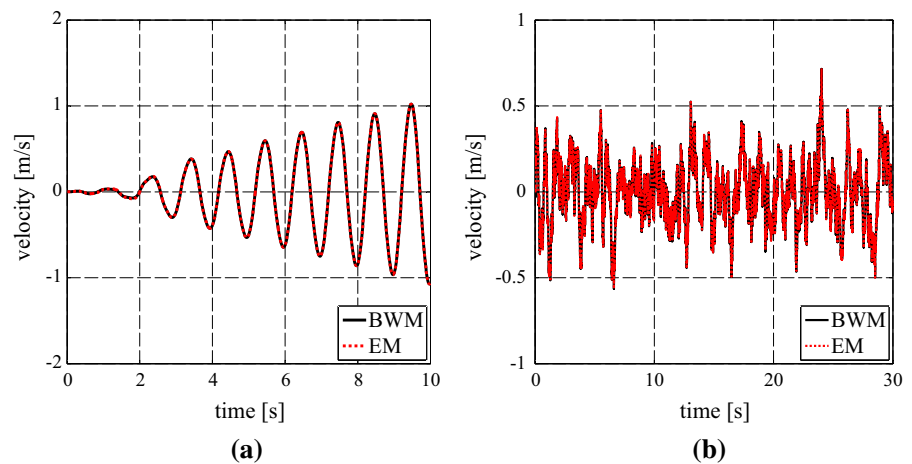


Fig. 14 Generalized acceleration time history obtained applying the **a** harmonic and **b** random force

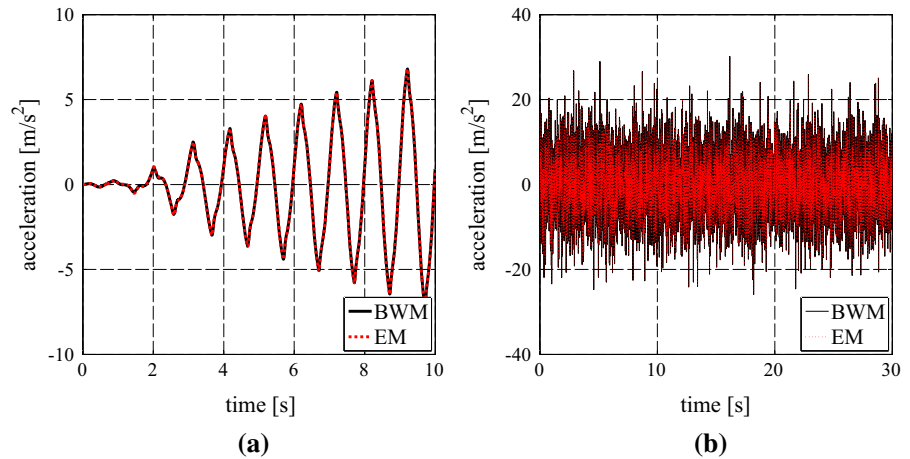
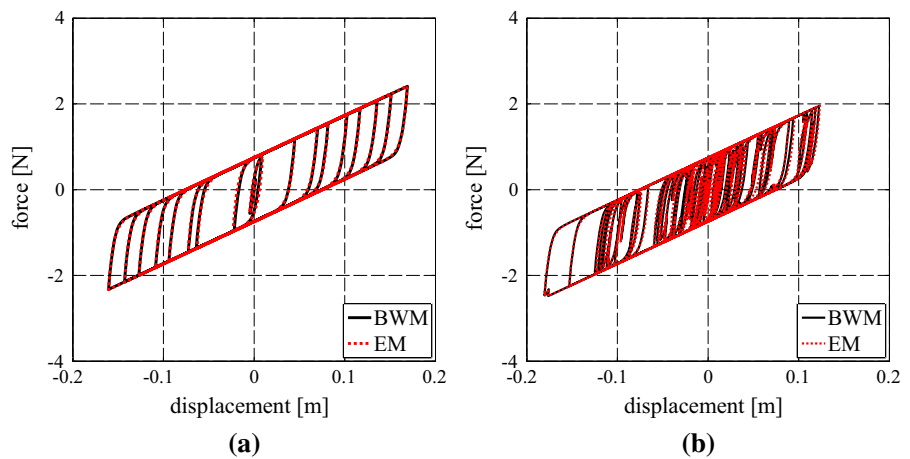


Fig. 15 Generalized force–displacement hysteresis loops obtained applying the **a** harmonic and **b** random force



been carried out on a rate-independent SDOF mechanical system with kinematic hardening behavior.

Both a harmonic and a random force have been considered in the analyses and the results of the EM have been compared with those associated with the celebrated BWM. In this respect, the following conclusions can be drawn:

- the results of the EM closely match those predicted by the BWM, independently of the kind of external force;
- the total computational time associated with the EM is equal to 0.66% (0.69%), for the harmonic (random) force case, of the one required by the BWM;
- the BWM requires the calibration of seven parameters to simulate hysteresis loops limited by two parallel straight lines, whereas the EM needs only three model parameters having a clear mechanical significance.

Current research activities, which will be the topic of future contributions, are focused on the parameters identification performed by gradient-based least square optimization algorithms, previously employed by the authors for similar purposes [20,62], and by static inverse identification [46]. Furthermore, current research is focusing on the extension of the proposed general formulation to the three-dimensional case through the definition of interaction domains involving loads and displacements. Such an approach has been successfully employed in characterizing non-linear materials by means of uniaxial relationships typically obtained from experimental tests, e.g., concrete [63], composites [21] or alloys [39]. Thus, using suitably defined interaction domains, one can infer equivalent load–displacement quantities which are related by

uniaxial relationships capable of determining equivalent flow rules.

Compliance with ethical standards

Conflict of interest The authors declare that they have no conflict of interest.

References

- Asano, K., Iwan, W.: An alternative approach to the random response of bilinear hysteretic systems. *Earthq. Eng. Struct. Dyn.* **12**(2), 229–236 (1984)
- Baber, T., Noori, M.: Random vibration of degrading, pinching systems. *J. Eng. Mech. ASCE* **111**(8), 1010–1026 (1985)
- Baber, T., Wen, Y.: Random vibration of hysteretic, degrading systems. *J. Eng. Mech. ASCE* **107**, 1069–1087 (1981)
- Bahn, B., Hsu, C.: Stress–strain behaviour of concrete under cyclic loading. *ACI Mater. J.* **95**(2), 178–193 (1998)
- Bathe, K.: *Finite Element Procedures*. Prentice Hall, Englewood Cliffs (1996)
- Bertotti, G.: *Hysteresis in Magnetism: For Physicists, Materials Scientists, and Engineers*. Academic Press, San Diego (1998)
- Besseling, J.: A theory of elastic, plastic, and creep deformations of an initially isotropic material showing anisotropic strain-hardening, creep recovery, and secondary creep. *J. Appl. Mech. ASME* **25**, 529–536 (1958)
- Bouc, R.: Modele mathematique d'hysteresis. *Acustica* **24**, 16–25 (1971)
- Carboni, B., Lacarbonara, W.: Nonlinear dynamic characterization of a new hysteretic device: experiments and computations. *Nonlinear Dyn.* **83**(1), 23–39 (2016)
- Carboni, B., Mancini, C., Lacarbonara, W.: Hysteretic beam model for steel wire ropes hysteresis identification. In: *Structural Nonlinear Dynamics and Diagnosis*, pp. 261–282, (2015)
- Caughey, T.: Random excitation of a system with bilinear hysteresis. *J. Appl. Mech. ASME* **27**(4), 649–652 (1960)
- Charalampakis, A., Koumousis, V.: Identification of Bouc–Wen hysteretic systems by a hybrid evolutionary algorithm. *J. Sound Vib.* **314**(3), 571–585 (2008)
- Coey, J.: *Magnetism and Magnetic Materials*. Cambridge University Press, Cambridge (2010)
- Dafalias, Y., Popov, E.: A model of nonlinearly hardening materials for complex loading. *Acta Mech.* **21**(3), 173–192 (1975)
- Dafalias, Y., Popov, E.: Cyclic loading for materials with a vanishing elastic region. *Nucl. Eng. Des.* **41**(2), 293–302 (1977)
- Dimian, M., Andrei, P.: *Noise-Driven Phenomena in Hysteretic Systems*. Springer, New York (2014)
- Dominguez, A., Sedaghati, R., Stiharu, I.: Modeling and application of mr dampers in semi-adaptive structures. *Comput. Struct.* **86**(3), 407–415 (2008)
- Duhem, P.: Die dauernden aenderungen und die thermodynamik. *i. Zeitschrift für Physikalische Chemie* **22**(1), 545–589 (1897)
- Elnashai, A., Izzuddin, B.: Modelling of material nonlinearities in steel structures subjected to transient dynamic loading. *Earthq. Eng. Struct. Dyn.* **22**(6), 509–532 (1993)
- Fedele, R., Sessa, S., Valoroso, N.: Image correlation-based identification of fracture parameters for structural adhesives. *Technische Mechanik* **32**(2), 195–204 (2012)
- Formica, G., Lacarbonara, W.: Three-dimensional modeling of interfacial stick-slip in carbon nanotube nanocomposites. *Int. J. Plast.* **88**, 204–217 (2017)
- Ghobarah, A., Korol, R., Osman, A.: Cyclic behavior of extended end-plate joints. *J. Struct. Eng. ASCE* **118**(5), 1333–1353 (1992)
- Giuffrè, A., Pinto, P.: Il comportamento del cemento armato per sollecitazioni cicliche di forte intensità. *Giornale del Genio Civile* **5**, 391–408 (1970)
- Greco, F., Raimondo, L., Serino, G., Vaiana, N.: A mixed explicit-implicit time integration approach for nonlinear analysis of base-isolated structures. *Ann. Solid Struct. Mech* (2017). DOI: 10.1007/s12356-017-0051-z.
- Gunston, T., Rebelle, J., Griffin, M.: A comparison of two methods of simulating seat suspension dynamic performance. *J. Sound Vib.* **278**(1), 117–134 (2004)
- Hauser, H.: Energetic model of ferromagnetic hysteresis. *J. Appl. Phys.* **75**(5), 2584–2597 (1994)
- Hodgdon, M.: Mathematical theory and calculations of magnetic hysteresis curves. *IEEE Trans. Mag.* **24**(6), 3120–3122 (1988)
- Ikhoulane, F., Hurtado, J., Rodellar, J.: Variation of the hysteresis loop with the bouc-wen model parameters. *Nonlinear Dyn.* **48**(4), 361–380 (2007)
- Iwan, W.: On a class of models for the yielding behavior of continuous and composite systems. *J. Appl. Mech. ASME* **34**(3), 612–617 (1967)
- Jiao, Y., Kishiki, S., Yamada, S., Ene, D., Konishi, Y., Hoashi, Y., Terashima, M.: Low cyclic fatigue and hysteretic behavior of u-shaped steel dampers for seismically isolated buildings under dynamic cyclic loadings. *Earthq. Eng. Struct. Dyn.* **44**(10), 1523–1538 (2015)
- Jiles, D., Atherton, D.: Ferromagnetic hysteresis. *IEEE Trans. Mag.* **19**(5), 2183–2185 (1983)
- Jiles, D., Atherton, D.: Theory of ferromagnetic hysteresis. *J. Appl. Phys.* **55**(6), 2115–2120 (1984)
- Kang, D., Jung, S., Nho, G., Ok, J., Yoo, W.: Application of bouc-wen model to frequency-dependent nonlinear hysteretic friction damper. *J. Mech. Sci. Techn.* **24**(6), 1311–1317 (2010)
- Krieg, R.: A practical two surface plasticity theory. *J. Appl. Mech. ASME* **42**(3), 641–646 (1975)
- Lacarbonara, W., Vestroni, F.: Nonclassical responses of oscillators with hysteresis. *Nonlinear Dyn.* **32**(3), 235–258 (2003)
- Laxalde, D., Thouverez, F., Sinou, J.: Dynamics of a linear oscillator connected to a small strongly non-linear hysteretic absorber. *Int. J. Non-Linear Mech.* **41**(8), 969–978 (2006)
- Lourenço, P., Ramos, L.: Characterization of cyclic behavior of dry masonry joints. *J. Struct. Eng. ASCE* **130**(5), 779–786 (2004)
- Lubliner, J.: *Plasticity Theory*. Macmillan, New York (1990)
- Majzoubi, G., Kashfi, M., Bonora, N., Iannitti, G., Ruggiero, A., Khademi, E.: Damage characterization of alu-

- minum 2024 thin sheet for different stress triaxialities. *Arch. Civ. Mech. Eng.* **18**(3), 702–712 (2018)
40. Manzoori, A., Toopchi-Nezhad, H.: Application of an extended bouc-wen model in seismic response prediction of unbonded fiber-reinforced isolators. *J. Earthq. Eng.* **21**(1), 87–104 (2017)
 41. Mayergoyz, I.: *Mathematical Models of Hysteresis*. Springer, New York (1991)
 42. Menegotto, M., Pinto, P.: Method of analysis for cyclically loaded r.c. plane frames including changes in geometry and non-elastic behavior of elements under combined normal force and bending. In: *Proceedings of IABSE Symposium on Resistance and Ultimate Deformability of Structures Acted on by Well-Defined Repeated Loads*, Lisbon, Portugal (1973)
 43. Nelson, R., Dorfmann, A.: Parallel elastoplastic models of inelastic material behavior. *J. Eng. Mech. ASCE* **121**(10), 1089–1097 (1995)
 44. Ok, J., Yoo, W., Sohn, J.: New nonlinear bushing model for general excitations using bouc-wen hysteretic model. *Int. J. Autom. Technol.* **9**(2), 183–190 (2008)
 45. Özdemir, H.: *Nonlinear transient dynamic analysis of yielding structures*. Ph.D. Thesis, University of California, Berkeley, CA, USA (1976)
 46. Pacitti, A., Peigney, M., Bourquin, F., Lacarbonara, W.: Experimental data based cable tension identification via nonlinear static inverse problem. *Proc. Eng.* **199**, 453–458 (2017)
 47. Piersol, A., Paez, T.: *Harris' Shock and Vibration Handbook*, 6th edn. McGraw-Hill, New York (2010)
 48. Quarteroni, A., Sacco, R., Saleri, F.: *Numerical Mathematics*. Springer, New York (2000)
 49. Ramberg, W., Osgood, W.: Description of stress-strain curves by three parameters. Technical Notes 902, National Advisory Committee on Aeronautics (1943)
 50. Rosenbrock, H.: Some general implicit processes for the numerical solution of differential equations. *Comput. J.* **4**, 329–330 (1963)
 51. Ru, C., Chen, L., Shao, B., Rong, W., Sun, L.: A hysteresis compensation method of piezoelectric actuator: model, identification and control. *Control Eng. Pract.* **17**(9), 1107–1114 (2009)
 52. Seo, J., Choi, I., Lee, J.: Static and cyclic behavior of wooden frames with tenon joints under lateral load. *J. Struct. Eng. ASCE* **125**(3), 344–349 (1999)
 53. Simo, J., Hughes, T.: *Computational Inelasticity*. Springer, New York (1998)
 54. Spizzuoco, M., Calabrese, A., Serino, G.: Innovative low-cost recycled rubber-fiber reinforced isolator: experimental tests and finite element analyses. *Eng. Struct.* **76**, 99–111 (2014)
 55. Subramaniam, P., Banerjee, S.: A correction to damping ratio for hyperbolic-hysteretic model for clayey soil. *Int. J. Geotech. Eng.* **7**(2), 124–129 (2013)
 56. Thomas, G., Weir, M., Hass, J., Giordano, F.: *Thomas' Calculus*, 11th edn. Addison Wesley Longman, London (2004)
 57. Tsai, C., Chiang, T., Chen, B., Lin, S.: An advanced analytical model for high damping rubber bearings. *Earthq. Eng. Struct. Dyn.* **32**(9), 1373–1387 (2003)
 58. Vaiana, N.: *Matlab codes for non-linear time history analysis of dynamic systems supported by wire rope isolators*. Master Thesis, 2nd level Master in Emerging Technologies for Construction, University of Naples Federico II, Naples, Italy (2015)
 59. Vaiana, N.: *Mathematical models and numerical methods for the simulation of the earthquake response of seismically base-isolated structures*. Ph.D. Thesis, University of Naples Federico II, Naples, Italy (2017)
 60. Vaiana, N., Serino, G.: Simulation of dynamic behavior of seismic isolators using a parallel elasto-plastic model. *WASET. Int. J. Civ. Environ. Eng.* **11**(2), 178–184 (2017)
 61. Vaiana, N., Spizzuoco, M., Serino, G.: Wire rope isolators for seismically base-isolated lightweight structures: experimental characterization and mathematical modeling. *Eng. Struct.* **140**, 498–514 (2017)
 62. Valoroso, N., Sessa, S., Lepore, M., Cricri, G.: Identification of mode-i cohesive parameters for bonded interfaces based on DCB test. *Eng. Fract. Mech.* **104**, 56–79 (2013)
 63. Valoroso, N., Marmo, F., Sessa, S.: A novel shell element for nonlinear pushover analysis of reinforced concrete shear walls. *Bull. Earthq. Eng.* **13**(8), 2367–2388 (2015)
 64. Visintin, A.: On hysteresis in elasto-plasticity and in ferromagnetism. *Int. J. Non-Linear Mech.* **37**(8), 1283–1298 (2002)
 65. Wen, Y.: Method for random vibration of hysteretic systems. *J. Eng. Mech. Divis. ASCE* **102**(2), 249–263 (1976)
 66. Wen, Y.: Equivalent linearization for hysteretic systems under random excitation. *J. Appl. Mech. ASME* **47**(1), 150–154 (1980)
 67. Wittke, H., Olfe, J., Rie, K.: Description of stress-strain hysteresis loops with a simple approach. *Int. J. Fat.* **19**(2), 141–149 (1997)
 68. Zaiming, L., Katukura, H.: Markovian hysteretic characteristics of structures. *J. Eng. Mech. ASCE* **116**(8), 1798–1811 (1990)
 69. Zhang, H., Foliente, G., Yang, Y., Ma, F.: Parameter identification of inelastic structures under dynamic loads. *Earthq. Eng. Struct. Dyn.* **31**(5), 1113–1130 (2002)
 70. Zona, A., Dall'Asta, A.: Elastoplastic model for steel buckling-restrained braces. *J. Constr. Steel Res.* **68**(1), 118–125 (2012)